Ultra-Short Echo Time Images Quantify High Liver Iron

Eamon K. Doyle ⓘ,[1,2] Kristin Toy,[3] Bertin Valdez,[2] Jonathan M. Chia,[4] Thomas Coates,[5] and John C. Wood[1,2]*

Purpose: 1.5T gradient echo-based R_2^* estimates are standard-of-care for assessing liver iron concentration (LIC). Despite growing popularity of 3T, echo time (TE) limitations prevent 3T liver iron quantitation in the upper half of the clinical range (LIC$\gtrless$20 mg/g). In this work, a 3D radial pulse sequence was assessed to double the dynamic range of 3T LIC estimates.
Theory and Methods: The minimum TE limits the dynamic range of pulse sequences to estimate R_2^*. 23 chronically-transfused human volunteers were imaged with 1.5T Cartesian gradient echo (1.5T-GRE), 3T Cartesian gradient echo (3T-GRE), and 3T ultrashort TE radial (3T-UTE) pulse sequences; minimum TEs were 0.96, 0.76, and 0.19 ms, respectively. R_2^* was estimated with an exponential signal model, normalized to 1.5T equivalents, and converted to LIC. Bland–Altman analysis compared 3T-based estimates to 1.5T-GRE.
Results: LIC by 3T-GRE was unbiased versus 1.5T-GRE for LIC $\leq$ 25 mg/g (sd = 9.6%); 3T-GRE failed to quantify LIC > 25 mg/g. At high iron loads, 3T-UTE was unbiased (sd = 14.5%) compared to 1.5T-GRE. Further, 3T-UTE estimated LIC up to 50 mg/g, exceeding 1.5T-GRE limits.
Conclusion: 3T-UTE imaging can reliably estimate high liver iron burdens. In conjunction with 3T-GRE, 3T-UTE allows clinical LIC estimation across a wide range of liver iron loads.
Magn Reson Med 79:1579–1585, 2018. © 2017 International Society for Magnetic Resonance in Medicine.

Key words: iron overload; relaxometry; UTE; T_2^*; Liver

INTRODUCTION

Chronic anemias such as thalassemia and sickle cell disease represent the most common genetic disorders in the world. Transfusion therapy in these patients produces severe iron deposition in the liver and other organs, leading to cardiac and endocrine dysfunction as well as liver cirrhosis. Iron overload in transfusional siderosis cannot be treated with phlebotomy; instead, patients receive iron chelators that bind and remove iron. Dosing must be adjusted based on tissue iron content, necessitating reliable iron quantitation techniques. Before 2005, needle biopsies were required to measure liver iron, with their attendant risks (1) and sampling error (2–4). Since then, magnetic resonance imaging systems have become important tools for diagnosing and monitoring iron overload disorders including sickle cell disease, thalassemia, hemochromatosis, and neurodegenerative disorders (5,6). Both transverse relaxivity and magnetic susceptibility measurements have been used to estimate tissue iron concentrations in the liver, heart, endocrine glands, and brain.

MRI-based iron quantitation at 1.5T is now standard of care (7). However, it is estimated that 50% of new magnet installations are 3T and some imaging centers use exclusively 3T magnets; this necessitates development of robust imaging techniques for high-field systems. Previous studies have validated quantitation over lower iron burdens at 3T (8–10). However, liver iron quantitation with high-field scanners (3T and above) remains limited by rapid signal decay. When increasing the field strength from 1.5T to 3T, field-dependent enhancement causes R_2^* ($1/T_2^*$) decay to approximately double, leading to transverse decay times below 0.5 ms in the liver, well below the range standard gradient-echo techniques can reliably capture (11). Inadequate sampling of rapidly decaying signal components leads to an underestimate of liver iron concentration (LIC). The development of ultra-short echo time (UTE) sequences has dramatically decreased the minimum achievable echo time (TE), enabling acquisition of ultra-fast decay species (12). UTE has shown promise to perform structural imaging of cartilage and bone. The reduced TE could potentially lead to significantly increased dynamic range in quantitative imaging approaches used to non-invasively estimate LIC at 3T and above. Proof of concept in this regard was published quite recently (13,14).

In this work, we measured liver R_2^* in human volunteers receiving treatment for transfusional iron overload using Cartesian gradient echo (GRE) and UTE sequences. We obtained 3T LIC estimates in milligrams of iron per gram of dry liver (mg/g) for comparison with clinical LIC estimates obtained at 1.5T using a previously derived relationship between liver R_2^* at 1.5T and 3T (11). We demonstrate that 3D radial UTE imaging increased the achievable dynamic range of LIC estimates to match, and possibly exceed, estimates from Cartesian gradient echo images obtained at 1.5T, providing a reliable means to quantify high liver iron at 3T.

Table 1
Relevant Scan Parameters.

Parameter	1.5T Gradient Echo	3T Gradient Echo	3T UTE
TEs (ms)	0.96–11.5; 16 linearly spaced	0.76–8.8; 16 linearly spaced	0.19, 0.23, 0.35, 0.60, 0.85, 1.0, 2.0
FOV (AP[cm] $\times$ RL[cm])	30 $\times$ 40	30 $\times$ 40	31 $\times$ 31
Slice (# $\times$ thickness[mm])	3 $\times$ 10	3 $\times$ 10	6 $\times$ 15
Matrix	84 $\times$ 84	84 $\times$ 84	88 $\times$ 88
TR (ms)/FA (deg)	50/30	50/30	5/4
Scan time (s)	14	14	5 per echo time/35 total
Breathhold (s)	14	14	None
Gradient strength	Max	Max	Max
Acceleration	No	No	TFE Factor 200

METHODS

Participant Population

Study participants were selected from a population of patients at the Children's Hospital of Los Angeles (CHLA) undergoing chronic transfusion therapy for sickle cell disease, thalassemia, and other rare anemia syndromes. Participants provided informed consent to participate in an IRB-approved study (CHLA Study CCI-14-00034). Each participant received a clinically indicated MRI assessment for iron overload on a 1.5T scanner followed by a research imaging protocol at 3T. Imaging data from a repeat clinical visit was available for a single participant and was weighted proportionally in resulting statistics.

Participant Assessment

Images were acquired on single-RF-transmit Philips Achieva 1.5T and 3T clinical scanners (software revision v3.2.2 or v5.1.7, Philips HealthTech, Best, Netherlands) using 16-element SENSE-XL torso coils. Clinical liver iron estimates were obtained from 1.5T R_2^* estimates using a 3-slice gradient echo acquisition, henceforth referred to as 1.5T-GRE. Two series—a 16-echo Cartesian gradient echo series (3T-GRE) and a set of seven single-echo, center-out, stack-of-stars, 3D radial images with varying echo times (3T-UTE)—were acquired at 3T. Compared to Cartesian gradient echo, center-out radial trajectories facilitate significantly reduced echo times by beginning readout from the center of k-space; the removal of the dephasing gradient prior to readout allows the echo to be acquired more quickly after excitation. 3T-UTE echo times were selected with approximate log spacing to maximize dynamic range. The minimum echo time of 0.19 ms was selected to facilitate quantitation of LIC $\geq$ 60mg/g; other scan parameters including gradient strength and slice thickness were selected to permit the shortest echo time. Relevant sequence parameters for all series are available in Table 1. All images were reconstructed on-scanner; the default reconstruction was used for 1.5T-GRE and 3T-GRE series while 3T-UTE images were reconstructed with the Philips SENSE implementation without undersampling. Clinical and research liver R_2^* estimates were made pixelwise in hand-segmented regions of interest encompassing the whole liver but avoiding large vasculature and biliary structures. R_2^* estimates were made by fitting an exponential + constant (exp + c) model (see Eq. [1]) to the data using Levenberg-Marquardt least squares minimization with previously-validated software developed at CHLA in MATLAB (Mathworks, Natick, MA) (9). The exp + c signal model, which was used to fit 1.5T-GRE, 3T-GRE, and 3T-UTE data, is as follows:

$$S(t) = S_0 e^{-R_2^* t} + c \qquad [1]$$

where $S(t)$ represents echo intensity at each echo time t, S_0 represents signal intensity at $t = 0$, R_2^* represents relaxation rate, and c represents noise bias and contributions from slow-decay species. The fitting model was chosen for all scans to allow for comparison of the 3T-UTE technique with our existing, clinically-established analysis toolbox (9). R_2^* estimates obtained at 3T were converted to 1.5T R_2^* equivalents using a previously-derived relationship (11):

$$R(Y) - R_{iY} = (R(1.5T) - R_{i1.5T}) * E_R(Y) \qquad [2]$$

$$E_{R_2^*}(B_0) = -0.0086 + 0.68 * B_0 \qquad [3]$$

where $R(Y)$ represents the relaxation rate R_2^* at a given field strength Y, R_{iY} represents the relaxation rate for normal liver at field strength Y, $E_R(Y)$ represents the relaxation rate enhancement for R_2^* from 1.5T to field strength $Y = B_0$ given by $E_{R_2^*}(B_0)$. Normal liver R_2^* values for 1.5T and 3T were assumed to be 31.1 and 44.4 Hz, respectively, based on internally derived estimates from healthy controls. These values, derived from a young cohort of patients, are similar to but slightly lower than previously published values derived in adults (8); this disagreement is expected based on the difference in age between the subject populations and the known increase in liver iron accumulation with age (15,16).

All LIC estimates were made using the 1.5T R_2^*-LIC calibration curve derived from biopsy (5). Bland–Altman analysis comparing 1.5T-GRE LIC estimates with 3T-UTE and 3T-GRE LIC estimates was performed; based on the expected failure of 3T-GRE techniques at high iron burdens, participants were assessed in two separate cohorts: LIC$\leq$25 mg/g and LIC > 25 mg/g.

Phantom

R_2^* estimates were validated in a phantom (0–24 mM $MnCl_2$ vials in a 0.25 mM $MnCl_2$ bath) constructed of
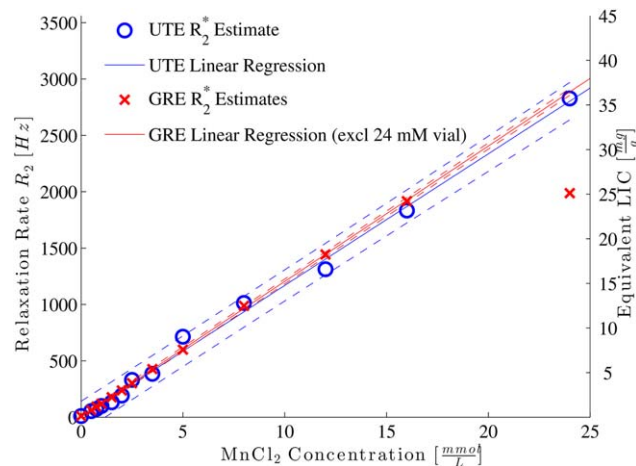
FIG. 1. Phantom results demonstrate linear correlation of $MnCl_2$ concentration and R_2^*. Regression analysis demonstrated the following relationships: R_2^*-UTE $= 117 \times$ [mM $MnCl_2$] $+ 1.6$ ($r^2 = 0.9955$, $r_{adj}^2 = 0.9951$, $P < 0.0001$); R_2^*-GRE $= 120 \times$ [mM $MnCl_2$] $+ 3.5$ ($r^2 = 0.9998$, $r_{adj}^2 = 0.9998$, $P < 0.0001$). The R_2^*-GRE regression excluded the highest-concentration vial due to expected failure of fitting. 95% confidence intervals are shown with dashed lines for each regression.

1/4-plexiglass sheet measuring $16.5'' \times 12.5'' \times 7.5''$. 100-mL Nalgene vials containing (0.0, 0.5, 0.75, 1.0, 1.5, 2.0, 2.5, 3.5, 5.0, 8.0, 12.0, 16.0, 24.0) mM $MnCl_2$ were suspended on the center line along the longest dimension or offset $2.25''$ laterally from the center line. Vials were staggered in a honeycomb layout to reduce inter-vial susceptibility effects. The phantom was imaged at 3T with the 3T-GRE and 3T-UTE protocols.

Simulation

A simulation evaluating the effects of proton-density fat fraction (PDFF) on $\exp + c$-derived LIC estimates was conducted. Signals were simulated by superposing water and a 6-peak fat model (17) with PDFFs of 0, 5, 10, and 20%. Decay was simulated as a mono-exponential and decay rates were calculated from a previously-derived LIC-R_2^* relationship (5,11) up to 45 mg/g. Noise was added to match an approximate first-echo SNR of 40 for images obtained in a normal liver. Signals for each LIC-PDFF combinations were simulated 20 times to provide pixelwise-like data and sampled at TEs matching the 3T-UTE and 3T-GRE protocols. Samples were fit using the same $\exp + c$ technique as imaging data, pixelwise-like-LIC estimates were averaged, and the resulting LIC error was determined.

Software

A historical repository containing snapshots of relevant code can be found at https://github.com/cornercase/snapshot_research_ute_vs_gre_LIC/releases/tag/v1.1 or via its DOI: 10.5281/zenodo.570291. (18)

RESULTS

Phantom

Analysis of phantom results (Fig. 1) demonstrated that the 3T-UTE and 3T-GRE protocols successfully quantified R_2^* up to 2830 and 1910 Hz, respectively, equivalent to LICs of 35.8 and 24.4 mg/g. The 3T-GRE results demonstrated failure in the highest concentration vial, showing saturation of R_2^* rather than the expected linear increase; the sample was excluded from analysis. No saturation was observed in the UTE data. Linear regression of 3T-UTE data gave the following relationship: R_2^* $_{3T-UTE} = 117 \times$ [mM $MnCl_2$] $+ 1.6$ ($r^2 = 0.996$, $r_{adj}^2 = 0.995$). Regression of 3T-GRE results demonstrated a similar linear relationship: R_2^* $_{3T-GRE} = 120 \times$ [mM $MnCl_2$] $+ 3.5$ ($r^2 = 0.999$, $r_{adj}^2 = 0.999$). The regressions show less than 3% disagreement in the slope of the R_2^*–$MnCl_2$ relationship.

Participant

A set of 24 imaging series were gathered from 23 participants (11M/12F, 21.5 ± 12.0 years, 11 Thalassemia Major, 8 Sickle Cell Disease, 4 other rare anemia, LIC $= 1.9$–40.7 mg/g); additional demographic information is summarized in Table 2. Subjects were generally lean, had a broad range of iron overload, and had mild transaminitis. Example images and R_2^* maps are demonstrated in Figure 2.

Figure 3 demonstrates the scatter plot of LIC estimates measured with 3T-UTE and 3T-GRE compared with LIC estimates from 1.5T-GRE; a line of unity is displayed for reference. The 3T-GRE data (represented by **X**) track the unity line until LIC exceeds 22 mg/g ($R_2^* \approx 1750$ Hz) and then plateau, similar to the plateau demonstrated by 24 mM $MnCl_2$ in Figure 1. In contrast, LIC by 3T-UTE (represented by ◯) tracks the unity line up to 40 mg/g. For some clinical iron estimates near 40 mg/g, the approximate upper limit of the 1.5T protocol, 3T-UTE produces higher iron estimates than 1.5T-GRE (see shaded region, Figs. 3 and 5).

The agreement between Cartesian GRE measurements at 3T and 1.5T is summarized by Bland Altman analysis (Fig. 4). For subjects with clinical LIC ≤ 25 mg/g (represented by ●), the 1.5T-GRE and 3T-GRE are unbiased with respect to each other with a standard deviation of 9.6%. Participants with LIC > 25mg/g (represented by ◯) demonstrated large bias ($37.3\% \pm 9.8$). The failure of 3T-GRE fits at high iron loads causes LIC by 3T-GRE to

Table 2

Ranges of Demographic and Laboratory Data for the Participant Population.

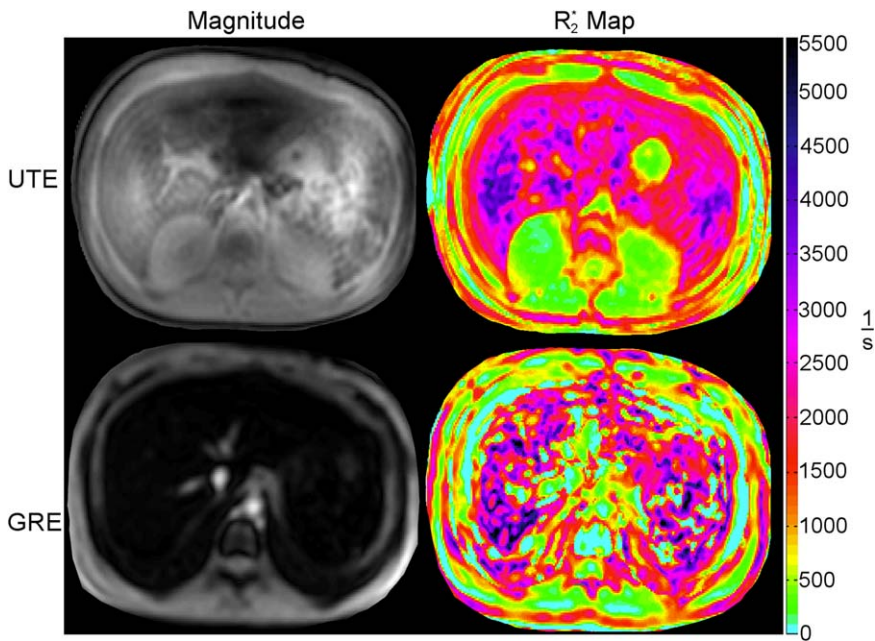| Measurement	Min	Max	Mean ± SD
Height (cm)	117	179.8	156.2 ± 15.3
Weight (kg)	20.1	89.7	54.3 ± 17.1
Body surface area (m²)	0.81	2.1	1.5 ± 0.3
Body mass index (kg/m²)	14.7	34.3	21.9 ± 5.1
Ferritin (ng/mL)	199	16,300	4483 ± 4890
ALT (U/L)	18	391	74.5 ± 84.5

FIG. 2. Example images demonstrating image quality of 3T-UTE (above) and 3T-GRE (below) first echo images and associated R_2^* maps. The image selected is from a subject with high LIC, causing the failure of the 3T-GRE protocol to capture sufficient signal to perform R_2^* estimation.

be uncorrelated with LIC by 1.5T-GRE, causing the bias to grow with the average of the two LIC estimates.

Figure 5 demonstrates the Bland Altman relationship between LIC derived from 3T-UTE versus 1.5T-GRE. For LIC > 25mg/g, 3T-UTE LIC estimates were unbiased with a standard deviation of 14.5%. For lower LIC values, UTE overestimated LIC compared to 1.5T-GRE by an average of 15.7% ± 21.9%.

Simulation

Simulation results demonstrated that physiologic amounts of liver fat cause estimates of LIC by 3T-UTE to overestimate liver iron compared to 3T-GRE. 3T-UTE error grows with PDFF but is relatively stable across iron loads above 5 mg/g. after an initial over-estimate of liver iron. Below 5 mg/g, error in LIC by 3T-UTE grows for all PDFFs, suggesting the maximum echo is too short for the 3T-UTE protocol to reliably quantify slow decay in the presence of noise, similar to the bias demonstrated in Figure 5. In contrast, the 3T-GRE protocol is relatively robust to fat effects until the signal decay approaches the upper limit of the dynamic range. Approaching the upper range limit, LIC by 3T-GRE overestimates LIC by up to 6% before failing. Results are further summarized in Supporting Figure S1.

DISCUSSION

Rapid decay rates have remained a persistent challenge for estimating high liver iron loads at 3T and higher field strengths. Iron quantitation in the heart and liver have been reported at 3T (19,20) with traditional cartesian gradient echo techniques and slice-selective, half-pulse UTE iron quantitation has been successful at 1.5T and 3T up to LICs of 35.4 mg/g ($R_2^* \approx$ 3200 Hz) (13). This is the first study to match the dynamic range of 1.5T-GRE sequences. Our existing 3T-GRE techniques offered excellent robustness up to 20–25 mg/g, though the exact limit is scanner-dependent due to differing software options that limit

echo spacing and first echo timing and hardware limitations such as coil blanking intervals and noise characteristics. The UTE protocol in this study was specifically designed to supplement an existing clinical quantitation workflow rather than replace it in order to maximize adoptability and permit the use of existing clinical tools without the need for algorithm or workflow changes. Both the phantom data (Fig. 1) and the human data (Figs. 3–5) suggest that the 3T-UTE can quantify R_2^* up to an LIC equivalent of ≥40 mg/g. UTE therefore nearly doubles the range of iron compared to the 1900 Hz (LIC≈24 mg/g) limit of our 3T-GRE sequence. Further, 3T-UTE may even
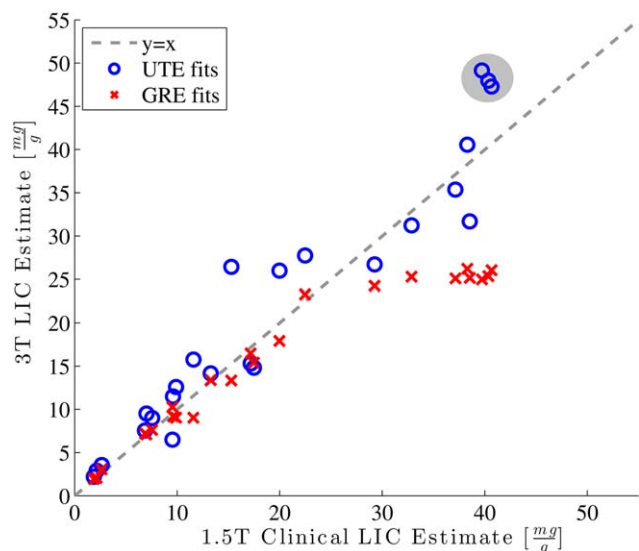

FIG. 3. Scatter plot demonstrating LIC estimates made with 3T GRE and 3T UTE image series compared with clinical estimates. Failure in LIC estimates is apparent in 3T GRE estimates for participants with clinical iron loads over 25 mg/g. Points in the shaded region demonstrate 3T-UTE LIC estimates that exceed the upper limit that 1.5T-GRE can quantify.
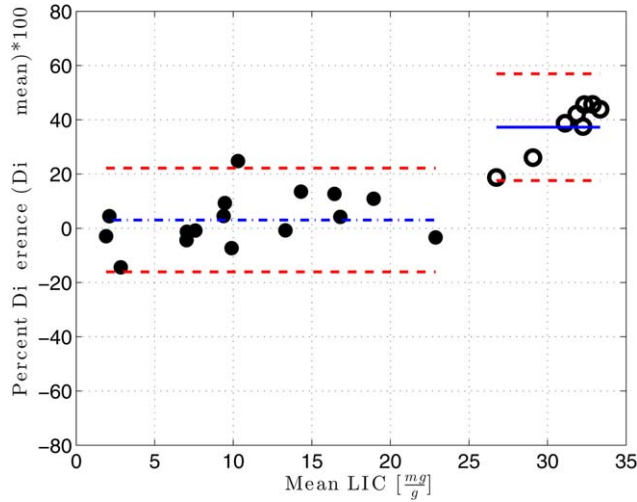
FIG. 4. Bland–Altman analysis of LIC estimates made with 1.5T-GRE and 3T-GRE series. Solid circles (●) represent participants with clinical LIC $\leq$ 25 mg/g ($\mu = 3.0$ (not significant), $\sigma = 9.6$). Unfilled circles (○) represent participants with clinical LIC >25 mg/g ($\mu = 37.3$, $\sigma = 9.8$). 95% limits of agreement are shown as dashed lines. Insignificant bias is demonstrated with a dash-and-dotted line. The bias demonstrated in the low-LIC cohort is thought to be a result of a lack of sufficiently long TEs in the UTE protocol; simulation results (supplemental results) for the 3T-UTE protocol in low LIC loads supports this conclusion.

exceed the dynamic range of the 1.5T-GRE protocol, quantifying R_2^* up to LIC$\geq$49.2 mg/g. Together, UTE and GRE at 3T in their current forms allow a comprehensive diagnostic alternative to 1.5T assessment.

Based on robust performance of 3T-GRE for low LIC quantitation (8), we optimized the 3T-UTE sequence for performance at iron loads over 20 mg/g. As such, we chose to acquire UTE data to a maximum TE of 2.0 ms. One downside of this approach is that only one fat oscillation was sampled. At 3T, out-of-phase fat oscillations can cause a substantial reduction in magnitude of the echoes between 0.5 and 1 ms. The combination of these fat oscillations and the 3T-UTE protocol's chosen echo times lead to non-obvious interactions with the $\exp + c$ fitting model (21), which assumes that the fat behavior can be sufficiently modeled by the bias term in Equation [1]. For LICs between 15 and 20mg/g, which demonstrate R_2^* decay rates between 1200 and 1800 Hz at 3T, the fat oscillations cause an apparent acceleration in R_2^* decay while the exponential decay suppresses fat oscillation data from the later echoes. This causes overestimation of R_2^* and artificially increases LIC from 3T-UTE between 15 and 20 mg/g. Over this range, the fat oscillations also interact unfavorably with the bias coefficient from Equation [1]. We found the $S(0)$-normalized bias, c, from Equation [1] tended to be 2–4 times larger for the 3T-UTE fit than the 3T-GRE fit over the LIC range of 15–20 mg/g; over the higher and lower LIC ranges, the bias values were similar. This behavior is consistent with previous studies (21). We speculate that extending 3T-UTE to longer echo times would improve the quantitation because the bias term will stabilize with increased oscillations.

The pixelwise $\exp + c$ fitting model (Eq. [1]) was selected based on its robustness, biopsy validation, and lack of strict protocol and data export requirements (5,22). Such considerations may be important in driving clinical adoption, especially when clinical facilities have difficulty acquiring or exporting phase information or hope to assess UTE images with established curve fitting workflows designed for Cartesian GRE techniques. Including spectral models of fat in the fitting algorithm may address the challenges related to bias while also allowing for the simultaneous estimation of tissue iron and fat content. This would overcome the 3T-UTE's previously-noted overestimation of LIC for moderate iron loads. However, this approach is more challenging due to stricter data and computational requirements (23). Further, the addition of fit parameters has been shown to increase the standard deviation of the R_2^* estimates (21). In certain clinical settings, it may be preferable to choose between the UTE and GRE estimates depending on the patient's expected iron load. In this case, models such as $\exp + c$, which lack explicit fat models, provide a reliable iron estimate; other fitting models such as truncated exponential (23) should work as long as appropriate R_2^*-LIC calibration curves are used (19,24). Though out of scope for this study, we speculate that R_2^* estimation with complex fitting techniques will meet or exceed the performance of the magnitude-based technique presented here.

Bland–Altman analysis of the 3T-UTE data shows that it is unbiased with respect to 1.5T-GRE estimates for LIC > 25 mg/g. Disagreement between 3T-UTE and 1.5T-GRE estimates for LIC 40 mg/g (shaded region, Figs. 3 and 5) suggest an improvement in the dynamic range
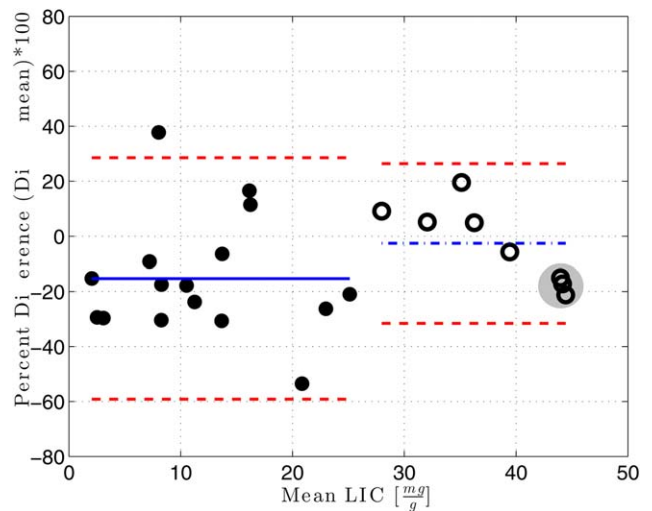

FIG. 5. Bland–Altman analysis of LIC estimates made with 1.5T-GRE and 3T-UTE series. Solid circles (●) represent participants with clinical LIC$\leq$25 mg/g ($\mu = -15.3$, $\sigma = 21.9$). Unfilled circles (○) represent participants with clinical LIC >25 mg/g ($\mu = -2.6$ (not significant) $\sigma = 14.48$). 95% limits of agreement are shown as dashed lines. Insignificant bias is demonstrated with a dash-and-dotted line. Points in the shaded region demonstrate 3T-UTE LIC estimates that exceed the upper limit that 1.5T-GRE can quantify.

from 3T-UTE compared to 1.5T-GRE rather than a failure of 3T-UTE. Though this could not be experimentally verified, the relationship between 3T-UTE and 1.5T-GRE was identical to the plateau observed between 3T-GRE and 1.5T-GRE; i.e., values exceeding the dynamic range "pile up." In retrospect, the study would have benefitted from UTE at 1.5T, as well, to accurately measure LIC > 40 mg/g. We have subsequently integrated 1.5T-UTE into our clinical protocol.

The clinical applicability of the UTE technique is further supported by its robustness to chest wall motion. In contrast to GRE sequences, which can show significant respiratory ghosting in free-breathing subjects, no coherent ghosts were visible in free-breathing UTE scans. The demonstrated robustness of the free-breathing protocol will immediately improve LIC estimates for participants who cannot complete a breath-hold of over 10 s. Patient comfort is improved through the negation of breath-holds and the reduction in scan time due to decreased protocol duration and reduction in repeated series. SNR improvement relative to breath-holding has been demonstrated with triggered, free-breathing UTE imaging (25) and improved R_2^* estimation in iron overloaded liver (14). In constrast, slice-selective UTE has demonstrated robustness in LIC up to $R_2^* \approx 1150$ Hz (13). Further studies will be needed to compare quantitative differences between free-breathing and breath-hold 3D UTE protocols in iron imaging.

Although many techniques that shorten TE compared to Cartesian sequences are considered UTE sequences (26), the term "UTE" is often associated with 2D imaging that achieves short echo times by combining data from two excitations with half-sinc pulses that use opposite slice-selection gradients (27). The shortened TE is achieved because readout takes place in the space traditionally occupied by the right tail of the sinc pulse. We previously attempted LIC quantitation on both Philips and GE magnets using half-pulse UTE but were unable to achieve reliable quantitation. We speculate that the severe off-resonance that occurs in iron-loaded livers, small timing inaccuracies, and slice-profile effects (12) led to the failure of this approach. Krafft and colleagues demonstrated that 2D UTE quantitation could be markedly improved by including adjacent saturation bands to suppress out-of-slice contributions and chemically selective spatial saturation of fat to suppress streak artifact (13). The downside of this approach is that it limits acquisitions to a single slice and alters the R_2^*-iron calibration, but it remains a viable alternative.

In contrast, 3D UTE techniques such as the one chosen for this study use a non-selective excitation pulse, which have demonstrated more reliable R_2^* quantitation in phantoms (12). The non-selective UTE pulse is high-bandwidth and has a lower duration than the half-sinc pulses used in slice-selective UTE, preventing off-resonance from causing under-excitation. 3D UTE also allows whole liver coverage in manageable imaging times.

Although this study focused on quantitation at 3T, the UTE protocol shows promise at other field strengths. Most notably, it may increase the dynamic range at 1.5T, resolving the demonstrated upper limit of 41 mg/g.

Further, the imaging challenges resulting from the near-linear increase of R_2^* with field strength will compound at higher field strengths. UTE imaging will likely be the best approach to quantify even low and moderate liver iron at higher field strengths such as 7T. We therefore expect that the UTE for iron quantitation will grow in popularity at all field strengths. UTE approaches may also be synergistic for fat-water separation techniques as well as abdominal QSM (28).

CONCLUSION

Non-selective, center-out radial UTE imaging is a robust supplement to GRE for quantifying liver iron at 3T. Our 3T-UTE protocol accurately tracked 1.5T-GRE LIC estimates up to 40 mg/g and potentially measures LICs as high as 50 mg/g. The UTE pulse sequence was available through a clinical science key on both software release 3.2.2 and 5.1.7 Philips scanners and did not require breath-holding. The 3T-UTE protocol functions as a turn-key replacement for GRE imaging in high-LIC participants at 3T. Further improvement to the protocol and fitting approach may allow UTE to measure low and moderate iron concentrations with the same accuracy demonstrated at high iron.

ACKNOWLEDGMENTS

REFERENCES

1. Angelucci E, Baronciani D, Lucarelli G, et al. Needle liver biopsy in thalassaemia: analyses of diagnostic accuracy and safety in 1184 consecutive biopsies. Br J Haematol 1995;89:757–761.
2. Ambu R, Crisponi G, Sciot R, et al. Uneven hepatic iron and phosphorus distribution in beta-thalassemia. J Hepatol 1995;23:544–549.
3. Emond MJ, Bronner MP, Carlson TH, Lin M, Labbe RF, Kowdley KV. Quantitative study of the variability of hepatic iron concentrations. Clin Chem 1999;45:340–346.
4. Villeneuve JP, Bilodeau M, Lepage R, Ct J, Lefebvre M. Variability in hepatic iron concentration measurement from needle-biopsy specimens. J Hepatol 1996;25:172–177.
5. Wood JC, Enriquez C, Ghugre N, Tyzka JM, Carson S, Nelson MD, Coates TD. MRI R2 and R2* mapping accurately estimates hepatic iron concentration in transfusion-dependent thalassemia and sickle cell disease patients. Blood 2005;106:1460–1465.
6. Stankiewicz J, Panter SS, Neema M, Arora A, Batt C, Bakshi R. Iron in chronic brain disorders: imaging and neurotherapeutic implications. Neurotherapeutics 2007;4:371–386.
7. Wood JC, Zhang P, Rienhoff H, Abi-Saab W, Neufeld E. R2 and R2* are equally effective in evaluating chronic response to iron chelation. Am J Hematol 2014;89:505–508.
8. Storey P, Thompson AA, Carqueville CL, Wood JC, de Freitas RA, Rigsby CK. R2* imaging of transfusional iron burden at 3t and comparison with 1.5t. J Magn Reson Imaging 2007;25:540–547.
9. Meloni A, Zmyewski H, Rienhoff HY, Jr, Jones A, Pepe A, Lombardi M, Wood JC. Fast approximation to pixelwise relaxivity maps: validation in iron overloaded subjects. Magn Reson Imaging 2013;31:1074–1080.
10. Alstiza Echeverra JM, Castiella A, Emparanza JI. Quantification of iron concentration in the liver by MRI. Insights Imaging 2011;3:173–180.
11. Ghugre NR, Doyle EK, Storey P, Wood JC. Relaxivity-iron calibration in hepatic iron overload: predictions of a Monte Carlo model. Magn Reson Med 2014;74:879–883.

12. Josan S, Kaye E, Pauly JM, Daniel BL, Pauly KB. Improved half RF slice selectivity in presence of eddy currents with out-of-slice saturation. Magn Reson Med 2009;61:1090–1095.

13. Krafft AJ, Loeffler RB, Song R, Tipirneni-Sajja A, McCarville MB, Robson MD, Hankins JS, Hillenbrand CM. Quantitative ultrashort echo time imaging for assessment of massive iron overload at 1.5 and 3 Tesla. Magn Reson Med 2017;78:1839–1851.

14. Tipirneni-Sajja A, Krafft AJ, McCarville MB, Loeffler RB, Song R, Hankins JS, Hil-lenbrand CM. Radial Ultrashort TE Imaging Removes the Need for Breath-Holding in Hepatic Iron Overload Quantification by R2* MRI. AJR Am JRoentgenol 2017;209:187–194.

15. Cook JD, Finch CA, Smith NJ. Evaluation of the iron status of a population. Blood 1976;48:449–455.

16. Puliyel M, Sposto R, Berdoukas VA, Hofstra TC, Nord A, Carson S, Wood J, Coates TD. Ferritin trends do not predict changes in total body iron in patients with transfusional iron overload. Am J Hematol 2014;89:391–394.

17. Hernando D, Liang ZP, Kellman P. Chemical shiftbased water/fat separation: a comparison of signal models. Magn Reson Med 2010;64:811–822.

18. Eamon Doyle. cornercase/snapshot_research_ute_vs_gre_lic: Post-acceptance revision. Zenodo 2017; Bibtex: eamon_doyle_cornercase/ snapshot_research_ute_vs_gre_lic:_2017.

19. Meloni A, Positano V, Keilberg P, et al. Feasibility, reproducibility, and reliability for the T*2 iron evaluation at 3 T in comparison with 1.5 T. Magn Reson Med 2012;68:543–551.

20. Alam MH, Auger D, McGill LA, et al. Comparison of 3T and 1.5T for T2* magnetic resonance of tissue iron. J Cardiovasc Magn Reson 2016;18:40.

21. Hernando D, Kramer JH, Reeder SB. Multipeak fatcorrected complex R2* relaxometry: Theory, optimization, and clinical validation. Magn Reson Med 2013;70:1319–1331.

22. Wood JC, Zhang P, Rienhoff H, Abi-Saab W, Neufeld EJ. Liver MRI is more precise than liver biopsy for assessing total body iron balance: a comparison of MRI relaxometry with simulated liver biopsy results. Magn Reson Imaging 2015;33:761–767.

23. He T, Gatehouse PD, Kirk P, Mohiaddin RH, Pennell DJ, Firmin DN. Myocardial T*2 measurement in iron-overloaded thalassemia: an ex vivo study to investigate optimal methods of quantification. Magn Reson Med 2008;60:350–356.

24. Garbowski MW, Carpenter JP, Smith G, Roughton M, Alam MH, He T, Pennell DJ, Porter JB. Biopsy-based calibration of T2* magnetic resonance for estimation of liver iron concentration and comparison with R2 Ferriscan. J Cardiovasc Magn Reson 2014;16: 40.

25. Gai ND, Malayeri A, Agarwal H, Evers R, Bluemke D. Evaluation of optimized breath-hold and free-breathing 3d ultrashort echo time contrast agent-free MRI of the human lung. J Magn Reson Imaging 2016;43:1230–1238.

26. Tyler DJ, Robson MD, Henkelman RM, Young IR, Bydder GM. Magnetic resonance imaging with ultrashort TE (UTE) PULSE sequences: Technical considerations. J Magn Reson Imaging 2007;25: 279–289.

27. Pauly, JM, Conolly, SM, inventors. Stanford University, assignee. 1992 Sep 22. Magnetic resonance imaging of short T.sub.2 species with improved contrast. United States patent US 5,150,053.

28. Hernando D, Levin YS, Sirlin CB, Reeder SB. Quantification of liver iron with MRI: state of the art and remaining challenges. J Magn Reson Imaging 2014;40:1003–1021.

SUPPORTING INFORMATION

Additional Supporting Information may be found in the online version of this article.

Fig. S1. Simulation of 3T-GRE and 3T-UTE echo times with 0, 5, 10, and 20% PDFF over an LIC range of 0.5–45 mg/g demonstrate that increasing fat fraction has a greater effect on R_2^* for the UTE sequence than the GRE sequence. In particular, the 3T-UTE overestimates LIC more as PDFF increases for a given LIC. Further, at low LIC, the simulations for PDFF = 0% indicate that LIC is overestimated when noise is present and the decay rate is slow. The magnitude of error due to physiologically realistic PDFF may explain the increased apparent measurement variation between GRE and UTE.